Politecnico di Torino

Master's Degree in Mechanical Engineering

Real-time monitoring of photoinduced 3D printing through ultrasound

Supervisor:
Prof. Ignazio Roppolo

Candidate:
Francesco Di Renzo

Co-supervisor:
Prof. Giuseppe Rosi

Academic Year 2023/2024

Considerate la vostra semenza:
fatti non foste a viver come bruti,
ma per seguir virtute e canoscenza.

Dante Alighieri, Inferno XXVI

Contents

List of Figures

1 ABSTRACT

The aim of this thesis work was to initiate a research process aimed at developing a real-time monitoring system for the Digital Light Processing (DLP) 3D printing technology. This monitoring system is based on the use of longitudinal ultrasonic waves to monitor changes in resin properties during the printing phase. The experiments conducted during this thesis work, which will be detailed in the following chapters, were carried out at the University of Paris-Est Créteil (UPEC) within the "Laboratoire Modélisation et Simulation Multi Echelle" (MSME).

Photopolymerization, i.e. a chemical process which involves the light-induced solidification of liquid resins, is the core process for DLP technology. This 3D printing method allows the production of solid artifacts from a composition of monomers and/or oligomers, through exposure to UV or visible radiation. Currently, in the commercial landscape, there is a lack of real-time monitoring systems for the polymerization process, which would allow for the timely detection of any defects, implementation of immediate corrections and an easier calibration of the process.

Ultrasound waves are sound waves that have higher frequency than human hearing ability. They are extensively used in the medical field to detect and diagnose internal conditions, including imaging of internal organs, and to monitor the health and development of the fetus during pregnancy. Beyond the medical world, ultrasound waves can be employed in the industry, for example on a very low power level, to clean and control fragile objects and to ensure that materials are free from defects without the main materials being destroyed. This ability to penetrate opaque materials makes ultrasound waves suitable to many different applications and highly valuable in many sectors.

In conclusion, the aim of this thesis has been to introduce ultrasound monitoring techniques within the context of additive manufacturing, laying the groundwork for the future development of this technology.

2 Additive Manufacturing

2.1 Introduction to Additive Manufacturing

Additive Manufacturing (AM) is an innovative technology that makes possible to produce objects with complex shapes in less time than the traditional manufacturing process, without tools or other equipment needed. Moreover AM can generate items with high complexity, which could be very difficult or even impossible to be manufactured by other conventional processes. [43]

Additive manufacturing uses data from computer-aided-design (CAD) software or 3D object scanners to control the hardware to deposit material, layer upon layer, in precise geometric shapes. As its name implies, additive manufacturing adds material to create an object. By contrast, when you create an object by traditional means, it is usually necessary to remove material through milling, machining, carving, shaping or other means. [16]

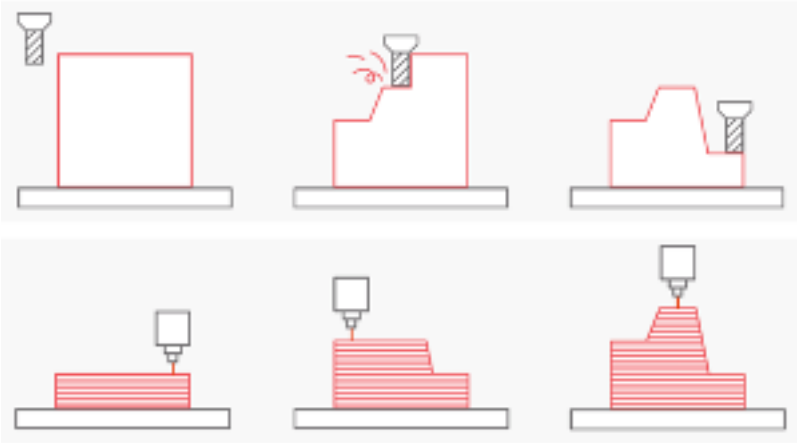

Figure 1: schematic representation of traditional manufacturing and additive manufacturing [31]

Additive Manufacturing technology was born in the 80s to reduce the time production of the prototypes and, due to this, for several years has been called "rapid prototyping". Despite the enormous developments in this sector, the manufacture of the prototype is still one of the major application of additive manufacturing.

Another expression used in the AM field is "3D printing" and generally associated with low cost processes, typically craft or hobbyist activities. The term "Additive Manufacturing" is instead used with reference to industrial production and manufacturing supply chains. Although the terms "3D printing" and "rapid prototyping" are casually used to discuss additive manufacturing, each process is actually a subset of additive manufacturing.

Such discussions have thus led to the definition of the term Additive Manufacturing (AM) as defined in ASTM F2792-12a standard (Standard Terminology for Additive Manufacturing Technologies) [40]. The term is universal and official, indicating all applications involving the use of a technology whose fundamental process is to join one or more materials to create objects, starting from 3D model data and overlaying one layer after another, unlike subtractive production technologies provided by traditional machine tools.

2.2 History and development of Additive Manufacturing

The first attempts to create solid objects using photopolymers date back to the late 1960s, but it wasn't until the early 1980s that the first practical application was seen. The first patent (US4575330) was filed by Chuck Hull in August 1984 for the Stereolithography (SLA) technology showed in figure 2 [27], which will be further discussed in the following paragraphs. By 1987, the technology was being used for prototyping and soon became a commercial reality. Other notable patents were that of "Fused Deposition Molting" technology (FDM) (US5121329) filed in 1989 by Scott Crump showed in figure 3 [6] and that of "Selective Laser Sintering" thechnology (SLS) (US4863538) by Carl Deckard [10].

Initially, these techniques were used only in the field of rapid prototyping, for the production of prototypes. This was because they allowed for much faster prototyping compared to traditional techniques. Moreover, they provided the ability to manufacture objects with complex geometries, which were difficult to achieve with other techniques, and customizable at low costs. From 1990 until the early 2000s, the primary use of AM technology in the industry field was in printing foundry patterns (rapid casting) or mold inserts (rapid tooling). The use of these 3D printing techniques in other industries was limited due to poor resolution and low availability of workable materials; in fact, with SLA only acrylate resins could be processed while with FDM only low-carbon thermoplastic polymers.

In recent decades, the development of new technologies in the field of AM has made possible the use of new types of polymeric materials and more recently metal, ceramic and fiber enriched composite components. In addition, the production volumes of AM machines are increasing more and more, making technology competitive from a cost point of view. Some of the sectors where Additive Manufacturing is currently used are: aerospace, medical and dental, automotive and jewelry.

2.3 Workflow for AM

The adoption of additive manufacturing techniques is subject to the availability of the mathematical model of the component created on a three-dimensional CAD system. Multiple steps are required to produce the 3D printed object, which are summarized in the figure 4. The first step is to design the part. This may involve to modify an existing design for AM or to start from scratch with a true design for additive manufacturing mindset. Computer simulation, generative design, and topology optimization can all be applied to optimize the function of the part. The printing process and material selection usually occur in the initial design step.

the universal standard in AM for the mathematical models is the file format STL (Standard Triangulation Language). The STL file was created in 1987 by 3D Systems Inc. when they first developed the stereolithography, and the STL file stands also for this term [46]. STL uses triangles to describe the surfaces to be built. Each triangle is described as three points and a facet normal vector indicating the outward side of the triangle. The STL file is used as a storage point for information concerning a 3D model. The information is stored in a format that offers a representation of the "raw" surface of the 3D model in triangles different sizes (depending on the required resolutions), as demonstrated by the Figure 5. At this stage, the process proceeds to slicing. The STL file is intersected with planes that are parallel to the z-axis and are separated by a defined distance, which subsequently determines the thickness of each material layer during printing. The data obtained from these sections are directly

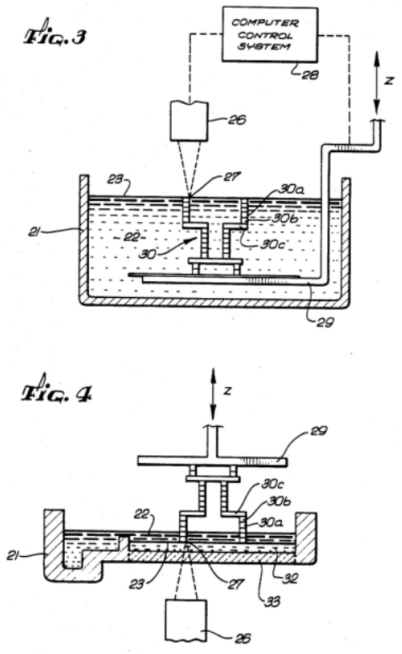

Figure 2: Stereolithography technology (patent US4575330) [27]

utilized by the additive manufacturing machine.

The following step is the planning of the build. Depending on the intended 3D printing technology, this step may entail selecting part orientation, adding support structures, packing or nesting multiple parts together, and setting printer parameters such as layer height, laser spot size, feed rate, etc.

at this point, the components are ready to be printed. A 3D printing build might take anywhere from minutes to days.

At the end of the building step, the components usually need to be post-processed. Depending on the process, post-processing could entail unpacking powder, prying or cutting parts from a build platform, cleaning, curing, heat treating, hot isostatic pressing, etc.

The last step is to finish the part. Many 3D printed tools and production parts will require further finishing to arrive at their completed state. Finishing steps might include machining surfaces, drilling or tapping holes, dyeing, coating or painting, and possibly welding or assembly with other parts.

Last but not least, inspection of the part is needed. Some parts can be evaluated with CMM (Coordinate Measuring Machine) measurement or 3D scanning; those with complex internal features may require X-ray or CT scanning (Computed Tomography). [37].

2.4 Advantages and Limitations of Additive Manufactruing

In this paragraph, additive and traditional technologies are compared, listing a series of key advantages and disadvantages of each. Some advantages of additive manufacturing compared to conventional processes are:

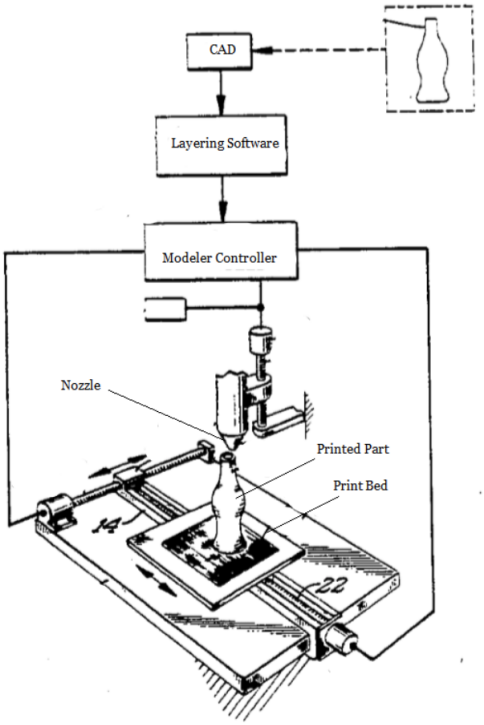

Figure 3: Fused Deposition Molting technology (patent US5121329) [6]

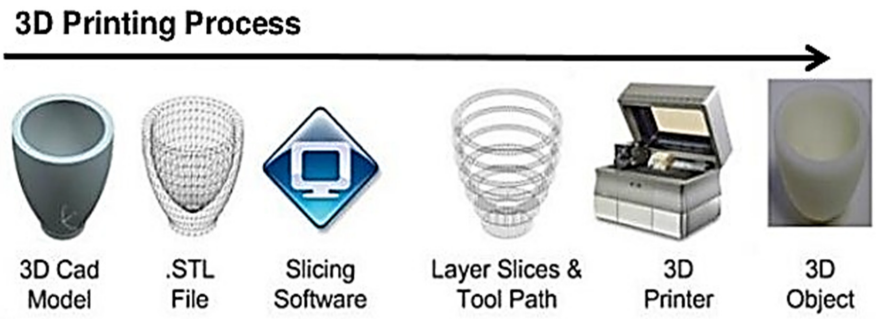

Figure 4: Three-dimensional printing process [32]

- The operational stages between the CAD model and the production of the part are reduced. The ability to print objects on demand is one of the key features of additive methodologies. Since the entire process relies on digital 3D models, these can be sent worldwide at nearly zero cost and printed at the desired location. This results in zero inventory and the replacement of physical warehouses with virtual ones, leading to significant cost savings.
- The human resources required for production control are reduced since the printing process is almost entirely automated.
- It is possible to produce a remarkable variety of geometric shapes, for instance,

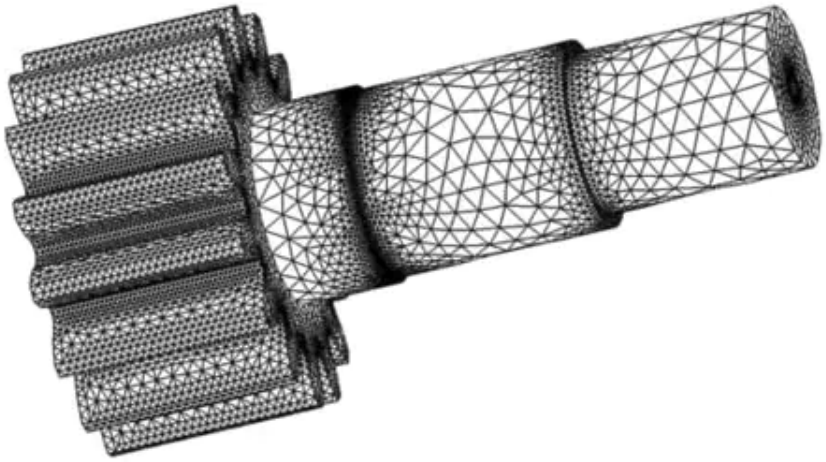

Figure 5: Surface triangulation of a gear wheel [39]

by manufacturing parts optimized from a topological standpoint, featuring internal grooves or undercuts that are impossible to achieve with traditional technologies.

- The cost of a component made with Additive Manufacturing does not increase (or increases minimally) with the complexity of the part to be printed, as illustrated in the figure 6. For component with simply geometry, conventional manufacturing is usually more affordable; but for complex geometry and, furthermore, if the component's design is optimized for AM, the production cost is lower compared to the same component made using subtractive techniques. [9].
- Additive Manufacturing demonstrates rapidity in producing small, intricately-shaped components, facilitating a reduction in material waste [23] and energy saving as well.
- It is possible to reconstruct damaged components of existing objects, based on the material of which the specific part to be restored is made [38] [3].

On the other hand, additive manufacturing presents some technological limitations both in terms of the process and regarding the product itself. Concerning the process:

- Work volumes are limited, primarily because the technology originated for prototyping purposes and later transitioned into the realm of final component production [46].
- Part sizes are limited by the dimensions of the machine [45].
- Inability to perform checks during the building process due to the absence of monitoring systems.
- Each machine can work with only a limited number of materials [18].
- Building speeds are limited [7].

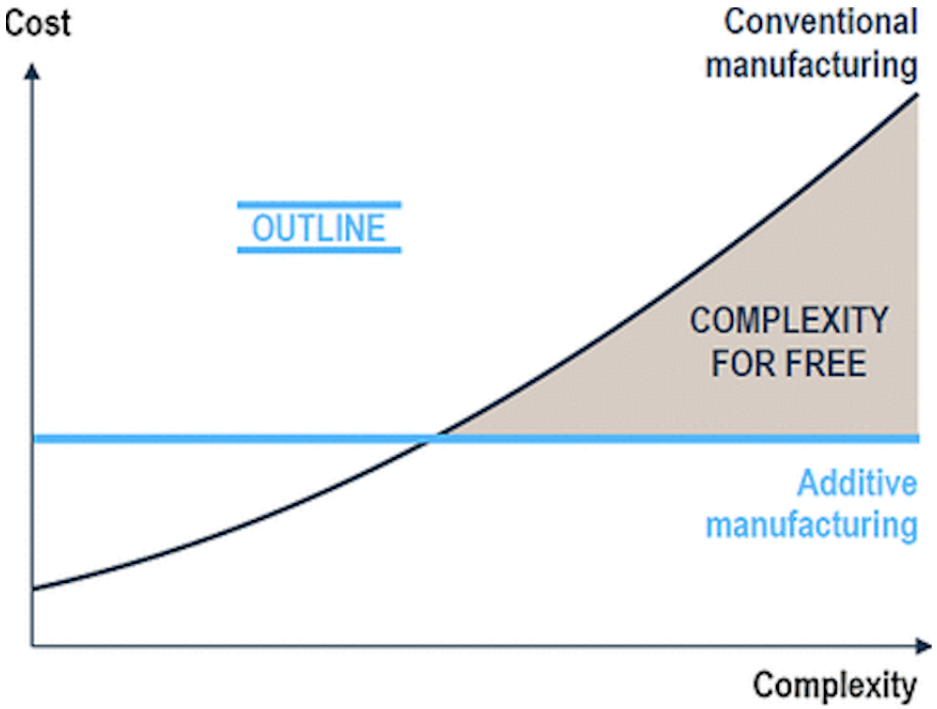

Figure 6: Cost and complexity comparison [9]

Regarding the product itself:

- Need for support structures during the printing phase to prevent damage to the part.
- Poor surface finish or not comparable to the finish achievable with traditional techniques.
- Limited availability of commercial materials.
- Material costs.

Rapid prototyping is still not the best solution for all cases, in some cases CNC (Computer numerical control) machining processes still need to be used.

2.5 Classification Additive Manufacturing technology

According to the American Society for Testing and Materials (ASTM F2792-12a), there are more than 50 different additive manufacturing technologies based on the above-classified processes [40] . Hence, ASTM has formulated a set of standards that classify the range of additive manufacturing processes into 7 general categories (ISO/ASTM 52900:2015). According to ASTM, based on the methodology of formation of the final components, AM processes can be classified into the following seven types, namely: jetting, binder jetting, vat photopolymerization, powder bed fusion, material extrusion, energy deposition and sheet lamination [2] (figure 7).

AM may be further classified based on the physical state of the base material used and processed to form the product. This classification includes solid, liquid, and powder-based processes (Figure 7).

- Solid-based techniques: these systems utilise solids as the primary media to create the part or prototype. To this category belong: FDM (Fused Deposition Modeling) technology, which utilizes the extrusion of a thermoplastic filament through a nozzle; LOM (Laminated object manufacturing) where several sheets of material are stacked and rolled together to form the desired object.

- Powder-based techniques: this technology is based on the use of material in powder form. Belong to this category technologies such as SLM (Selective Laser Melting) or EBM (Electron Beam Melting) for metal powder and SLS (Selective Laser Sintering) for polymeric powder. The powder is spread in thin layers and then fused using a laser in the case of SLM or SLS and with electron beam in EBM technology.

- Liquid-based techniques: in these techniques, a photocurable resin consisting of photopolymers and a photoinitiator undergoes photopolymerization upon exposure to appropriate light irradiation, resulting in rapid solidification. These procedures, also referred to as "vat photopolymerization techniques", precisely because the starting liquid resin is placed inside a vat, do not necessitate high temperatures and are characterized by their speed and simplicity. Digital Light Processing (DLP) falls under this category. In this technique the resin undergoes polymerization when exposed to ultraviolet radiation emitted by a projector. DLP will be explained in detail since it was used in this Thesis work. The Stereolithography (SLA), which it was introduced in the in previous pages, belongs to the liquid based category but the resin curing is made throughout laser beam. This technique will also be illustrated in detail in the following paragraphs, in order to give a clearer vision of the main differences that exist between these two AM techniques.

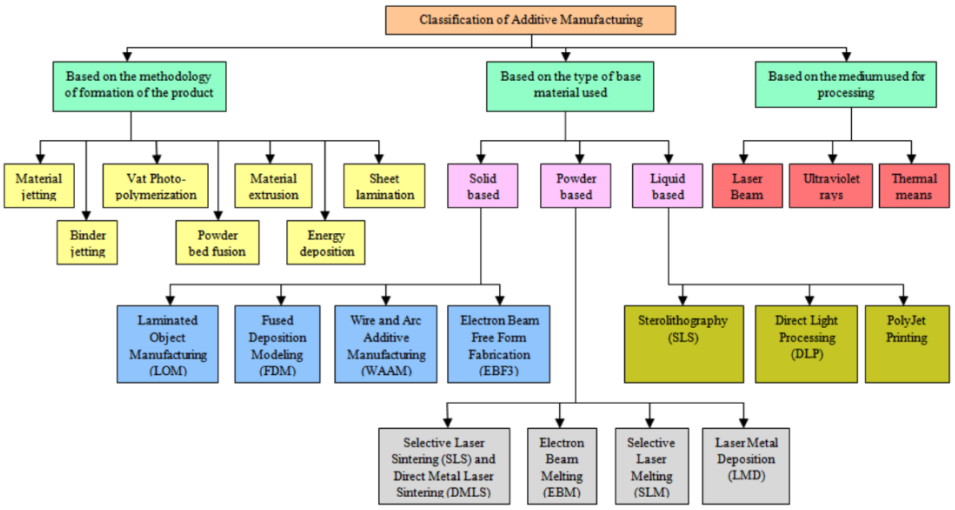

Figure 7: Classification of additive manufacturing processes from different contexts [2]

2.5.1 Stereolithography

Stereolithography (SLA), pioneered by 3D Systems, Inc., stands as the premier and most extensively employed method in rapid prototyping. Historically, the two terms were often interchangeable. This technique, rooted in a liquid-based approach, revolves around the curing or solidification of a photosensitive polymer upon exposure to an ultraviolet laser interacting with the resin. The workflow commences with a model crafted within CAD software, subsequently translated into an STL file delineating each layer as "slices" containing pertinent data. The thickness of these layers, as well as the overall resolution, hinge upon the apparatus utilized. A platform is fashioned to secure the object and provide support for any protruding features. The UV laser then selectively solidifies designated areas of each layer. Upon completion of a layer, the platform descends, and at the culmination of the process, excess material is drained for potential reuse. SLA printers are appreciated for their ability to produce objects with very fine details and smooth surfaces, making them ideal for applications that require precision and aesthetic quality, such as jewelry modeling, rapid prototyping, and engineering part production [43]. Figure 8 illustrates the fundamental components of a stereolithography machine.

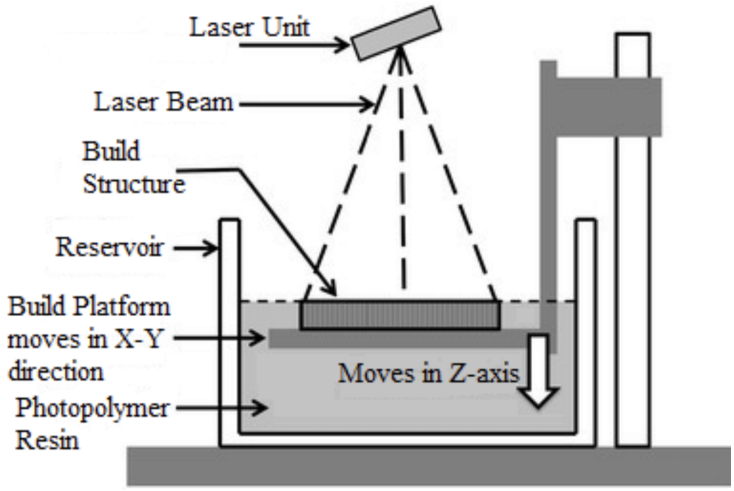

Figure 8: Schematic diagram of SLA printer configuration [43]

2.5.2 Direct Light Processing

Direct Light Processing (DLP) is an additive manufacturing technique for polymers and is part of the liquid-based technology group, where the raw material is supplied in the form of liquid resin and is polymerized using a UV projector. Due to the resin being in liquid state before polymerization, this technology allows for excellent performance in terms of dimensional tolerances and surface roughness.

As can be observed in figure 9, in contrast to SLA (Stereolithography), the component printed in DLP is usually inverted and anchored to the print platform (also using supports if necessary), which moves from bottom to top during component printing. The tank containing the resin has a transparent bottom allowing the light emitted by the projector to reach the resin. Thanks to this bottom-to-top approach, it is much

easier and more precise to manage the thickness of each individual printing layer compared to SLA technology, where the polymerized layer is on the surface, requiring a series of techniques to avoid resin rippling during platform movement.

The fact that the layer exposed to radiation is at the bottom of the tank allows this process to completely isolate the resin from contact with oxygen, ensuring better printing results.

A notable aspect is that in DLP, polymerization of the resin layer occurs simultaneously at all points of interest as the light source projects the image of each layer onto the resin in a single operation. In contrast, in SLA, the resin is illuminated point by point by the laser. This approach allows DLP printing to be faster, but at the same time tends to have lower resolution compared to SLA, especially in areas further from the center of the print platform.

After polymerization of each layer, the print platform moves upward, allowing more liquid resin to fill the space between the transparent bottom and the previously printed layer. This cycle repeats until the model is fully realized. Furthermore, compared to Stereolithography, the tank used in DLP is less deep, significantly reducing overall operating costs [30] [20] [35].

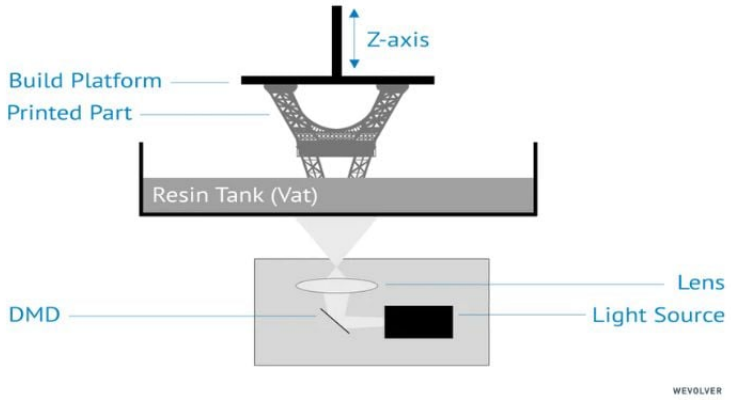

Figure 9: Direct Light Processing operating diagram [44]

2.5.3 DLP main defects

Since invented, DLP has evolved with significant improvement in speed, resolution, and cost. Despite being an advanced technology in the 3D printing field, several defects may occur during printing. One of the most common issues is the lack of adhesion to the build platform, which can cause the model to detach during printing, compromising the integrity of the final product (figure 10). Additionally, incomplete fabrication of structures is a frequent defect: parts of the model may be partially formed or missing, often due to errors in managing printing parameters or resin distribution (figure 11). Another significant problem is overexposure: if the resin is exposed to the light source for too long, areas of the model can become over-cured, resulting in surface deformations or overly rounded details, thus affecting the precision and quality of the final model (figure 12).

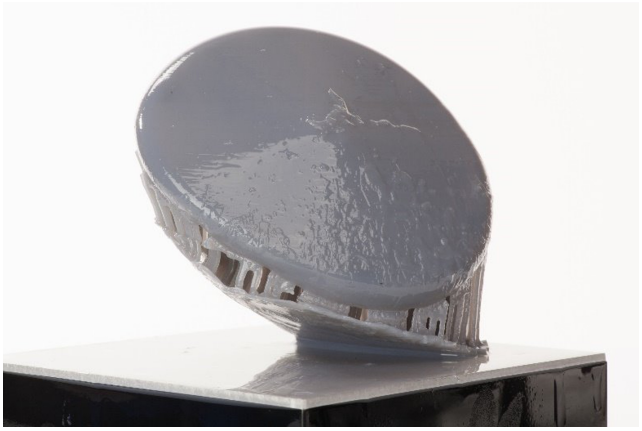

Figure 10: No adhesion on the building platform

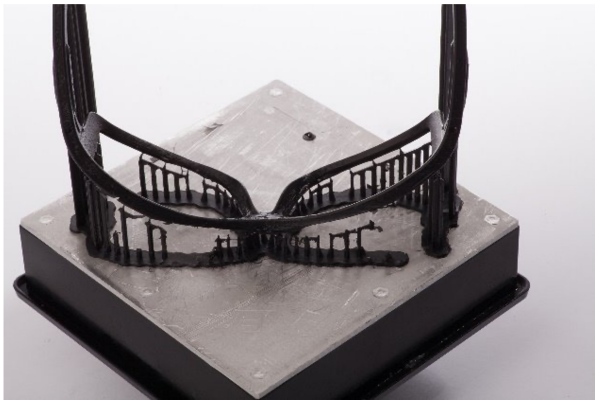

Figure 11: Incomplete fabrication of the structure

Figure 12: Over exposure

2.6 Non-Destructive Testing (NDT)

Non-Destructive Testing (NDT) is used to collect information about a material in ways that do not alter it (i.e., without destroying it).

Various techniques are employed in non-destructive testing to gather diverse sets of data, each demanding specific tools, training, and preparation. Some of these methods facilitate comprehensive volumetric inspections of objects, while others are tailored for surface inspections exclusively. Similarly, the efficacy of certain NDT methods can vary depending on the materials they are applied to, with some techniques, such as Magnetic Particle NDT, being applicable only to materials that can be magnetized [11].

The following are the eight most commonly utilized NDT techniques:

- Visual NDT (VT)
- Ultrasonic NDT (UT)
- Radiography NDT (RT)
- Eddy Current NDT (ET)
- Magnetic Particle NDT (MT)
- Acoustic Emission NDT (AE)
- Dye Penetrant NDT (PT)
- Leak Testing (LT)

The use of mechanical resonances to test properties of materials is older than the industrial revolution. Early documented cases of British railroad engineers tapping the wheels of a train and using the sound to detect cracks perhaps marks the first real use of resonances to test the integrity of high-performance alloys [25]. Ultrasonic Testing typically relies on sound waves to identify flaws or irregularities present within a material.

Among the prevalent Ultrasonic Testing methodologies is the pulse echo technique. In this approach, examiners introduce sound waves into a material and gauge the echoes generated by surface imperfections as they rebound back to a receiver.

The technology of ultrasonic wave propagation has proven to be a versatile and effective technique for monitoring and characterizing thermosetting resins during the curing process. This technique measures sound velocity and attenuation, parameters that are highly sensitive to changes in the viscoelastic characteristics of resins during curing. For instance, in monitoring the cure state of thermosetting resins, the sound velocity is related to the storage modulus and density of the resin, while the attenuation is associated with energy dissipation and scattering, making this technique particularly useful for observing the physical transformations occurring during the curing process [22].

Phase transformations, such as gelation and vitrification of unsaturated polyester resins, have been studied using high-frequency dynamic mechanical analysis through ultrasonic wave propagation. The increase in longitudinal sound velocity and the increase in sound attenuation are respectively attributed to the increase in longitudinal modulus and irreversible viscous losses, with a clear correspondence between these variations and the observed phase transformations [21].

Furthermore, ultrasonic wave propagation has been applied for the dynamic mechanical characterization of epoxy matrices for composites. During the curing process, ultrasonic wave propagation enables the calculation of complex longitudinal bulk moduli, with the evolution of attenuation and velocity closely related to the significant

physical changes occurring. In particular, ultrasonic velocity (or the longitudinal bulk modulus) emerges as a key parameter for cure monitoring, as it reflects the growth and evolution of the mechanical stiffness of the resin. The results suggest that the measurement of longitudinal velocity could be exploited for online measurements of post-gel properties, with an immediate correlation between gel time, the end of cure, and the ultrasonic data [24].

These studies highlight the reliability of ultrasonic wave propagation for monitoring the physical changes taking place during the curing of thermosetting resins, offering significant potential for online monitoring of the effectiveness of 3D printing process of photocurable resins, as well as the presence of printing defects (e.g. voids or cracks) during the processing of polymers and polymer matrix composites.

3 Ultrasound

3.1 Applications of Ultrasound

Ultrasounds are high frequency sound waves, with frequencies larger than those audible to the human ear, typicality 20 kHz. However, the frequency range employed in NDT it is between 1 and 10 MHz, as it is possible to observed in figure 13. These waves can be used in a wide range of applications, thanks to their properties of penetration, reflection, and diffusion. An area where ultrasounds find application is medicine. In medicine, they are used in diagnoses and treatment of a variety of ailments. For instance, medical imaging of the inner tissues of the body is possible through ultrasounds. This method effectively diagnoses untimely stages of diseases related to the heart, kidneys, and liver.

From a purely technical ultrasonic standpoint, there are many similarities between NDT and medical ultrasonics. Basically, one is attempting to locate defects in an opaque object; the same technological approaches are relevant, such as discriminating between closely spaced echoes and digging signals out of the noise. Respiratory effects, blood flow, and possible tissue damage are issues that are totally absent in NDT [8].

Applications of ultrasound in medicine for therapeutic purposes have been accepted and beneficial uses of ultrasonic biological effects for many years. Low-power ultrasound of about 1 MHz has been widely applied since the 1950s for physical therapy in conditions such as tendinitis and bursitis. In the 1980s, high-pressure-amplitude shock waves came into use for mechanically resolving kidney stones, and "lithotripsy" rapidly replaced surgery as the most frequent treatment choice. The use of ultrasonic energy for therapy continues to expand, and approved applications now include uterine fibroid ablation, cataract removal (phacoemulsification), surgical tissue cutting and hemosta- sis, transdermal drug delivery, and bone fracture healing, among others [26].

Ultrasounds are also applied to various industries. For example, distance measurement and detection of defects in materials, for example, cracks in pipes or metal structures; this technique is greatly exploited in aerospace, where the safety of the structures is the fulcrum. Another field of application of ultrasounds is cleaning. In fact, ultrasounds are used to clean delicate objects such as jewelry, watches, and medical equipment. This technique is particularly useful since it does not damage objects and does not need the use of aggressive chemicals. Ultrasound has also a wide range of applications in materials chemistry, primarily exploiting the chemical effects derived from acoustic cavitation. Bubble collapse in liquids results in an enormous concentration of energy from the conversion of the kinetic energy of the liquid motion into heating of the contents of the bubble [42].

Some of the main applications include:

- The sonochemical decomposition of volatile organometallic precursors in low-volatility solvents produces nanostructured materials. These materials can take various forms and exhibit high catalytic activities.
- Production of Nanostructures: Nanostructured metals, alloys, oxides, carbides, and sulfides, nanometer colloids, and nanostructured supported catalysts can be created using ultrasound.

Ultrasounds are also used in the food industry, for instance, equipment cleaning and the detection of flaws on foodstuff products. For example, ultrasounds can be used in detecting if there is a foreign body in food products, say seeds or stones.

Recently, ultrasound has been used to develop various effective and reliable applications for food processing. The most common applications in the food industry include cell destruction and intracellular material extraction. Depending on its intensity, ultrasound is used for enzyme activation or deactivation, mixing and homogenization, emulsification, dispersion, preservation, stabilization, dissolution and crystallization, hydrogenation, meat tenderization, ripening, aging and oxidation, and as an aid for solid-liquid extraction to accelerate and improve the extraction of active ingredients from different matrices, as well as degassing and atomization of food preparations [14].

Finally, they are used in the environmental field, for example, for detection of gas leaks in tanks and pipelines and measure water quality. Ultrasound technology plays a crucial role in gas leak detection, according to Moon et al. in "Ultrasound Techniques for Leak Detection" [28], its application for detecting leaks within vehicle cabins and pressure vessels has proven effective and versatile. Ultrasound waves, typically classified with spectral content above 20 kHz, offer significant advantages in terms of speed and accuracy compared to more traditional, time-consuming methods that can be invasive. Using high-frequency microphones, active methods employing ultrasonic emitters, passive techniques relying on airflow through leak points, and vibro-acoustic methods utilizing small electro-dynamic shakers are employed. These methodologies show promise in enhancing reliability and efficiency in quality control testing, while also reducing required testing times in production environments [28].

In summary, ultrasounds are a versatile technology, having wide applications in these different areas. With its gentle; yet very effective, properties, it gives the ability for ultrasounds to be applied for medical diagnosis, cleaning objects, defect detection in materials, and the measurement of water and air quality.

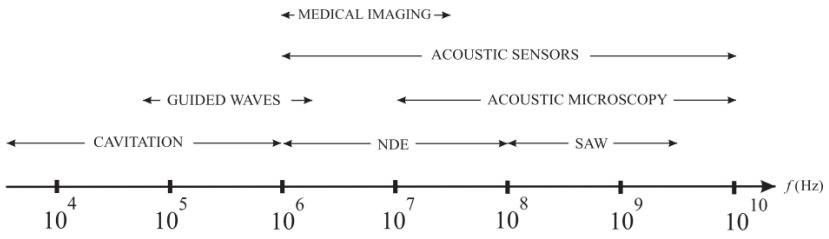

Figure 13: Common frequency ranges for various ultrasonic processes [8]

3.2 Harmonic Waves

In general a wave is defined as "the self-sustaining propagation at the constant velocity of a disturbance without change of shape"[8].
In a non-dissipative media, the one dimensional wave equation for a generic field $u(x,t)$ reads

$$\frac{\partial^2 u(x,t)}{\partial x^2} = \frac{1}{c^2}\frac{\partial^2 u(x,t)}{\partial t^2} \tag{1}$$

where c is the wave speed.

A general solution of the wave equation can be written as

$$u(x,t) = f(x-ct) + f(x+ct) \tag{2}$$

where $f(x-ct)$ and $f(x+ct)$ are the wave functions corresponding to progressive or regressive waves, respectively. A progressive wave is defines as a wave that propagates towards the increasing direction of the x axis.

The other relevant parameters involved in wave propagation are

- wavelength $\lambda = 2\pi/k$
- wave number $k = \omega/c$
- period $T = 1/f$
- frequency $f = \omega/2\pi$.

3.2.1 One dimensional wave equation for a viscoelastic material

Since this thesis will use longitudinal waves for monitoring polymerization, it is necessary to use appropriate nomenclature for the wave equation description. For longitudinal waves, the displacement vector is parallel to the direction of propagation. The displacement u is the component of the displacement vector along the wave propagation direction. In a viscoelastic material, the wave equation must take into account the dissipation effects and viscoelastic properties of the material. The equation (1) can be modified as follows:

$$\frac{\partial^2 u(x,t)}{\partial t^2} = \frac{E'}{\rho}\frac{\partial^2 u(x,t)}{\partial x^2} - \frac{E''}{\rho}\frac{\partial}{\partial t}\frac{\partial^2 u(x,t)}{\partial x^2} \tag{3}$$

In frequency domain, this equation can be rewritten in the following form

$$-\omega^2 U(x,\omega) = \frac{E^*}{\rho}\frac{\partial^2 U(x,\omega)}{\partial x^2}. \tag{4}$$

where

- $u(x,t)$ is the longitudinal displacement field and $U(x,\omega)$ is the corresponding Fourier transform.
- ρ is the material density.
- $E^* = E' + iE''$ is the complex elastic modulus, with E' (storage modulus) and E" (loss modulus).

- $c = \sqrt{\frac{E'}{\rho}}$ is the speed of the elastic wave in the material (dependent from the storage modulus).

If we consider a progressive plane wave propagating in the direction x, we can look for a solution like:

$$u(x,t) = Ae^{i(kx-\omega t)} \tag{5}$$

where A is a complex constant. The effects of attenuation are normally incorporated by using a complex wave number $k = \beta - i\alpha$. Using this solution in equation 4 we have that

$$k^2 = \frac{\rho\omega^2}{E^*} \tag{6}$$

Then, 5 become:

$$u(x,t) = Ae^{i((\beta-i\alpha)x-\omega t)} = Ae^{-\alpha x}e^{i(\omega t-\beta x)} \tag{7}$$

The attenuation coefficient α is given by the imaginary part of k:

$$\alpha = k_i = \frac{\omega E''}{2\sqrt{\rho E'}}. \tag{8}$$

The important result here is that the attenuation of the wave is proportional to the ratio of the loss modulus E" and the square root of the storage modulus E':

$$\alpha \propto \frac{E''}{\sqrt{E'}}$$

and the wave velocity is proportional to E':

$$c \propto \sqrt{E'}.$$

3.3 Measure of wave velocity and dissipation

There are several types of ultrasonic waves that can travel through solid media. These include longitudinal waves, shear waves, Rayleigh waves, or surface acoustic waves, and Lamb waves or plate waves. In longitudinal waves, material alternates between local compression and expansions. Material particles carrying the waves move in the same direction of the wave propagation.

Since gases and liquids are practically incapable of transmitting shear, for ultrasonic cure monitoring, longitudinal waves are normally preferred to shear waves, which present a very high level of attenuation in liquids and soft gel samples [21].

Ultrasonic waves differ in wavelength, amplitude of displacement, and velocity of propagation. In most applications, ultrasonic waves are generated with a transducer, which converts electrical energy into ultrasonic waves. The same transducer (or a second one) will convert the ultrasonic wave back to an electrical signal for further analysis [12]. In this work, the acoustic characteristics of a material are determined by two parameters, the ultrasonic velocity and the ultrasonic attenuation coefficient, α.

3.3.1 Ultrasonic Velocity

The velocity of propagation of elastic waves, determined by the "time of flight" (TOF) measurement, indicating how long it takes for sound to traverse a sample. This velocity of sound in a uniform substance correlates directly with its elastic modulus and density [21].

As previously illustrated in the paragraph 3.2.1, the wave speed is proportional at the square root of the storage modulus E':

$$c \propto \sqrt{E'}$$

Consequently, alterations in elasticity or density will invariably impact the time it takes for a pulse to move through a sample of consistent thickness.

TOF technique consists of measuring through how long a sound wave takes to travel through a material.

The main steps to follows to calculate the TOF are:

- Sample preparation: The sample has to be properly prepared with parallel surfaces so that the sound wave travels without much hindrance.
- Selection of transducer: An ultrasonic transducer is selected to generate the wave. It is detected with a receiver. In this example following, the same transducer can act as the emitter and receiver.
- Sound wave generation: A pulse is emitted from the transducer through the sample.
- Detection of the sound wave: The wave that has passed through the sample will then be detected by the receiver. The time between the pulse being emitted and the signal being received is called time of flight.
- Time of flight Measurement: The measurement of time of flight, with the aid of a data acquisition system, records the time the wave was input and the time it was received.
- Calculation of speed: From the definition, one can compute the speed of sound propagation, c, in the sample with the formula: $c = \frac{d}{t}$; where d is the distance traveled by the sound wave in the sample (the length of the sample) and t is the measured time of flight.

For demonstration purposes, a measurement of wave propagation within a sample with a thickness of $L = 45.82\,\text{mm}$ was carried out. In this example, a shear probe generating shear waves was used, but the procedure for calculating the time of flight remains the same even in the case of longitudinal waves. The configuration used is illustrated in Figure 14.

In Figure 15, the signal generated by the wave due to its propagation and reflection within the sample can be seen. Each peak shown in Figure 15 represents the wave that has traversed the sample, reflected at the bottom, and returned to the probe. For greater clarity, a space-time graph was created using COMSOL, illustrated in Figure 16, which allows for visualization of the wave's path during its propagation. In this graph, the slope of the lines represents the wave's propagation speed, which is influenced by the material used. Since, in this case, the material is always the same, the slope is constant. The wave propagates through the material, reflecting

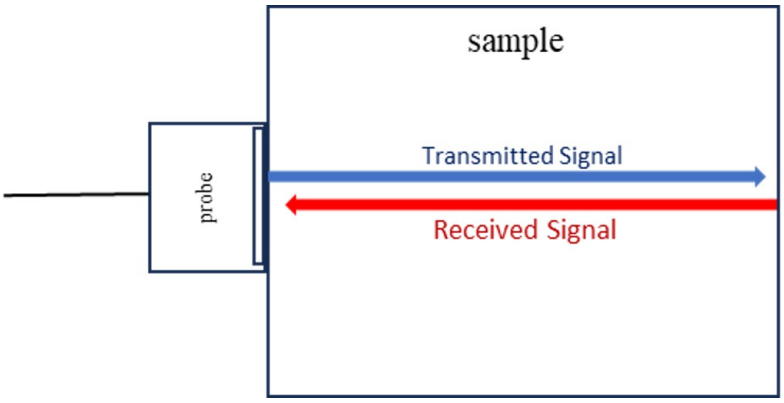

Figure 14: schematic configuration of weave propagation

at the bottom of the sample after about 15 microseconds. Subsequently, it returns, undergoing another reflection around 30 microseconds, this time at the left side of the sample (where the probe is positioned). The probe detects this second reflection as the first signal, highlighted by the first peak observable in Figure 8. This phenomenon repeats periodically until the signal completely dissipates.

By using the time-of-flight information between the various peaks and knowing the geometry of the components, it is possible, for example, to determine the wave propagation speed.

- $T_1 = 31.9\,\mu s$ - the instant in time when the probe detects the first peak in figure 15.
- $T_2 = 60.62\,\mu s$ - the instant in time when the probe detects the second peak in figure 15.

Since the distance traveled by the wave is $d = 2 * L$, we obtain:

$$c = \frac{d}{T_2 - T_1} = 3190.80\,\mathrm{m/s}$$

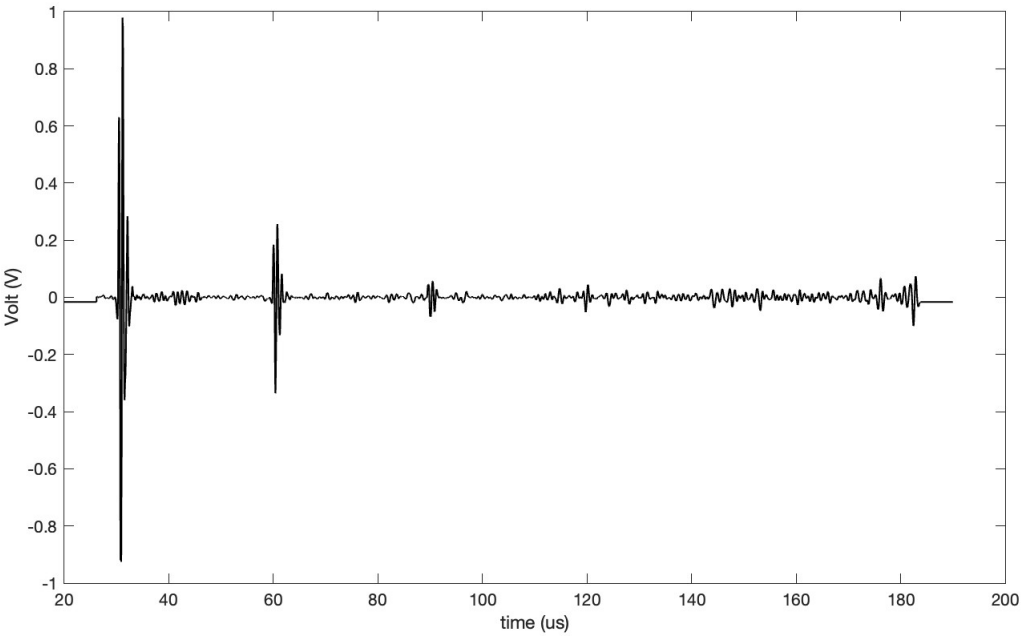

Figure 15: wave signal detected from the probe

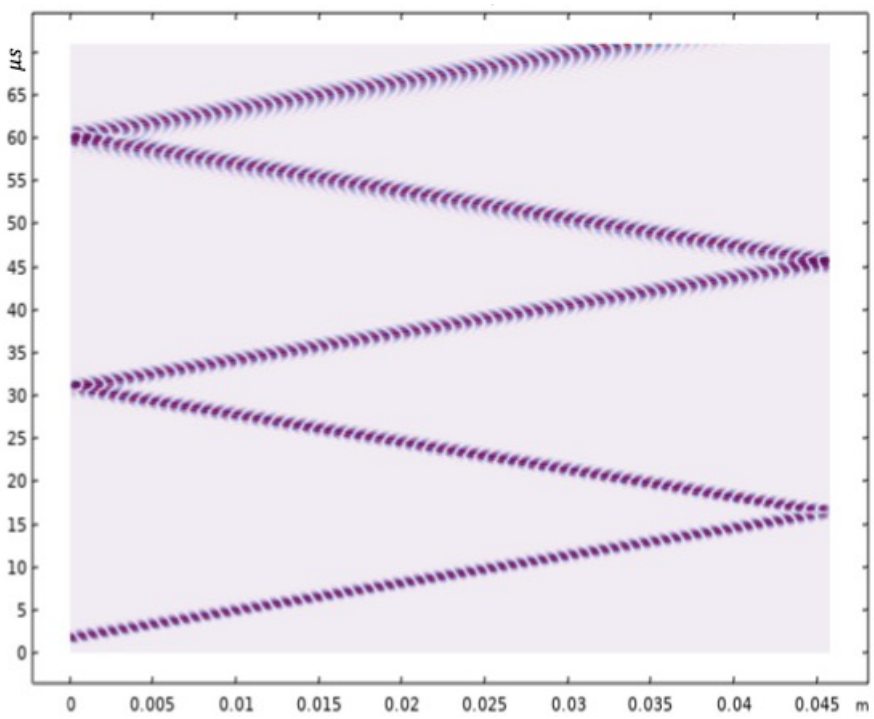

Figure 16: Simulation in COMSOL of the wave propagation in the sample

3.3.2 Ultrasonic Attenuation Coefficient

The attenuation is a measure of dissipative energy, converted to heat, as the wave propagates through the material. In addition to reflection losses at macroscopic defects

or other material discontinuities, most of the energy loss results from the absorption and the scattering of ultrasonic waves [21].

From the relation 8, the attenuation of the wave is proportional to the ratio of the loss modulus E" and the square root of the storage modulus E'.

$$\alpha \propto \frac{E''}{\sqrt{E'}}$$

When the energy of the signal is concentrated around a finite time interval, especially if its total energy is finite, one may compute the energy spectral density. More commonly used is the power spectral density (or simply power spectrum). The power spectral density (PSD) then refers to the spectral energy distribution that would be found per unit time, since the total energy of such a signal over all time would generally be infinite. Integration of the spectral components yields the total power [19]. By monitoring the total power of the received signal during the experiment in this manner, we can measure the energy dissipated during the polymerization reaction.

Calculating the power spectrum of an ultrasonic signal using MATLAB is a process that involves the Fourier transform of the signal. The power spectrum represents the distribution of the signal's energy as a function of frequency.

To monitor the variation of energy over time, the area under the power spectrum (P1) of each subsequent measurement is compared with that of the initial measurement. Using MATLAB's "trapz" function to calculate the area is appropriate because it integrates the signal value using the trapezoidal method. The main steps used to measure dissipation are illustrated below:

- Acquisition of the ultrasonic signal.
- Loading the signal into MATLAB.
- Computation of the FFT (Fast Fourier Transform): The Fourier transform is used to convert the signal from the time domain to the frequency domain. MATLAB's fft function makes this process simple.

  Y = fft(signal); % Calculating the FFT

- Normalizing and calculating the magnitude of the FFT (P1).

  P1 = abs(Y/N); % Normalizing the FFT

  with N = Number of signal samples.

- Calculating the power spectrum for each measurement

  $$PowerSpectrum = P1^2;$$

- Calculating the area under the power spectrum: the "trapz" function is used to calculate the area under the power spectrum curve for each measurement.
- Comparing the area of the initial measurement with the areas of subsequent measurements to determine the variation in energy. The comparison is made by taking the ratio of the area at the beginning of the measurement to the areas of the subsequent measurements.

Following these steps, it is possible to analyze how the energy of the ultrasonic signal varies over time, calculating the energy dissipation with respect to the initial state.

4 Materials and Methods

4.1 Principle of Photopolymerization

The technique underlying technologies such as DLP and SLA for solidifying a liquid resin and generating 3D components is Photopolymerization. The first Additive Manufacturing technology that employed this technique was stereolithography (SLA). Photopolymerization is a well-known process of polymerization induced by light irradiation, which offers several interesting advantages (such as high speed and stereo specificity), making it attractive for application in the additive industry [15].

The Photopolymerization process occurs after irradiation with light in the ultraviolet, visible, or near-infrared region of the spectrum, according to the photoinitiator absorption characteristics. Those are molecules that, absorbing the radiation, generate reactive species (such as radicals or cations) that react with the functional groups present in the monomer, propagating polymerization. Photopolymerizable formulations, including 3D printable formulations, are typically liquid and composed of various ingredients that will be introduced later [15]. (Metha)crylates are the monomers/oligomers most commonly used for this type of printing, and polymerization occurs through a radical system.

Radical systems involve three main phases: generation, propagation and termination of radicals. Radical generation in photopolymerization occurs under light irradiation, where a photoinitiator or a photoinitiator system is responsible for converting the light energy into reactive species to initiate photopolymerization. Most commercially available photoinitiators undergo the Norrish type I $\alpha - cleavage$ reaction and generate radical fragments under light irradiation [4]. The structures of common photoinitiators are presented in the figure 17.

(Meth)acrylate-based resins are compatible with various types of commercially available 3D printers and custom 3D printers. These resins have been used in various contexts such as 3D printing of shape memory polymers [47], highly elastic photopolymers [5], and functional materials for bio-applications [41].

The most common (meth)acrylate monomers/oligomers used in 3D printing include: PEGDA (the one used in this thesis), urethane-dimethacrylate (UDMA) , triethylene glycol dimethacrylate (TEGDMA), bisphenol A-glycidyl methacrylate (Bis-GMA), trimethylolpropane triacrylate (TTA) [15].

Although showing great effectiveness, (meth)acrylate-based resins do present some limitations for 3D photopolymerization: among others, shrinkage phenomena during polymerization may actuate deformations and layer manufacturing issues. The seriousness of this phenomenon depends on the molecular structure used as the monomer/oligomer. In order to contrast this problem, a number of strategies have been adopted. For instance, increasing the molecular weight of the oligomeric acrylates while decreasing the concentration of less reactive groups will generally reduce the percentage of shrinkage. However, to lower the high viscosity of these resins during the 3D printing process, heating is necessary [29].

Name	Chemical Structure	Light absorption (λ_{max})	Ref.
Benzophenone		253 nm	124
Phenyl bis (2,4,6-trimethylbenzoyl) phosphine oxide (BAPO, Irgacure 819)	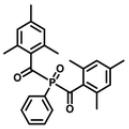	295 nm, 370 nm	14,20,36,50,115
2-hydroxy-2-methyl-1- phenyl-propan-1-one (Irgacure 1173)	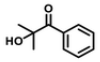	245 nm, 280 nm, 331 nm	36
2-Hydroxy-4′-(2-hydroxyethoxy)-2-methylpropiophenone (Irgacure 2959)	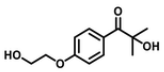	274 nm	9,28,50,116,125–127
2,2′-azobis[2-methyl-n-(2-hydroxyethyl) propionamide] (VA-086)	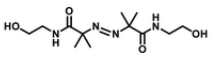	375 nm	118–121
2,2-dimethoxy-2-phenylacetophenone (Irgacure 651 or DMPA)	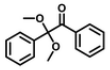	252 nm, 340 nm	50,128,129
Diphenyl(2,4,6-trimethylbenzoyl)phosphine oxide (Darocure TPO; Lucirin TPO)	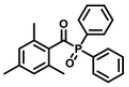	295 nm, 368 nm, 380 nm, 393 nm	20,114,122
lithium phenyl(2,4,6-trimethylbenzoyl)phosphinate (LAP)	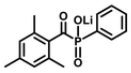	375 nm	25,27,121,130–133
Ethyl (2,4,6-trimethylbenzoyl) phenylphosphinate (Lucirin TPO-L)	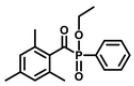	275 nm, 379 nm	39,134

Figure 17: Chemical structures of common UV light photoinitiators used in 3D photopolymerizationsSystems [4]

4.2 3D printable formulations

These formulations typically involve components like monomers/oligomers and photoinitiators (PI), often supplemented with additional substances such as radical scavengers, dyes, fillers, or additives for specific printing improvements [1].

The choice of monomers considers such factors as the way they operate, thickness, speed of reaction and final product properties. All the chemicals used in this thesis were purchased by Merck (Italy) and used without purification.

The matrix used in this thesis work was Poly(ethylene glycol) diacrylate with a molecular weight of 250 Da (PEGDA 250, figure 18).

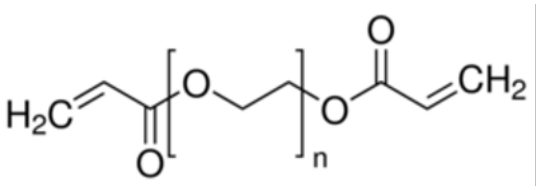

Figure 18: PEGDA's structure [34]

In the Vat Polymerization (VP), light triggers a photoinitiator which transforms liquid monomers into a solid network. It is important to select the appropriate photoinitiator and balance the composition of the material so that it can cure fast and that light can penetrate deeply. This affects the printing speed, accuracy, and strength. There are several photoinitiators present in the market that activate at different wavelengths such as ultraviolet (UV), visible light (VIS) and near-infrared (NIR). Most radical photoinitiators absorb light in the ultraviolet and visible ranges, compatible with all vat polymerization techniques, particularly DLP, which often utilizes light emitted at 405 nm.

The photoinitiator used was Phenylbis(2,4,6-trimethylbenzoyl)phosphine oxide (BAPO, figure 19).

The formulations employed for preliminary testing were prepared by adding the monomeric resin and the photoinitiator to test tubes in an amount equivalent to 2% by weight of the monomer. Subsequently, the dispersion of the photoinitiator was enhanced through the utilization of an ultrasonic bath.

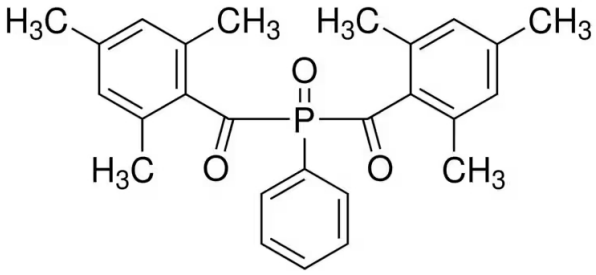

Figure 19: BAPO's structure [33]

Another resin used in this thesis work was BioMed Clear. BioMed Clear Resin is a rigid material for biocompatible applications requiring long-term skin or mucosal membrane contact. This USP Class VI certified material is suitable for applications that require wear resistance and low water absorption over time [13]. Being a commercial resin, its composition is non provided.

4.3 Gel Point and Rheological Curves

Gelation (gel trasition) is defined as the phase transformation during which the curing resin transforms from a viscous liquid to an elastic gel, the viscosity of the system increase and the shear response of the resin grows from zero to finite values. The propagation reaction is triggered by the interaction of the initiator with the radiation who will react and turn into a radical. Branched polymers can establish connections between chains, resulting in progressively larger polymers. As reaction proceed, larger branched polymers are formed, and at a certain stage, covalent cross linking bonds between the macro molecules are generated. At this stage of reaction, known as the gel point, the system loses fluidity, and viscosity significantly increases. The onset of gelation, or gel point, is marked by a sudden viscosity spike.

Typically, the kinetics of polymerization and the formation of polymerization crosslinking are measured during UV polymerization using a rotational rheometer. This directly identifies the development of the gel network structures. As example, in Figure 20, rheological curves are presented showing the rheological evolution of the storage modulus (G') during the photopolymerization process of PEGDMA [17].

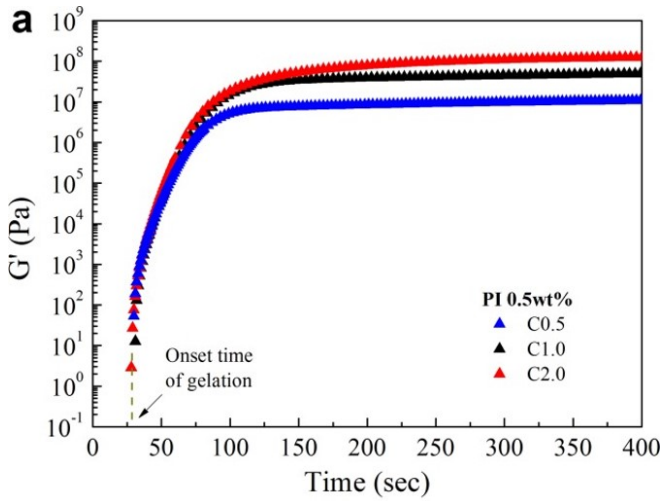

Figure 20: examples of rheological curves (PEGDMA) [17]

One of the most common methods to identify the gel point is the analysis of the crossover frequency between the storage modulus G' (elastic modulus or storage modulus) and the loss modulus G" (viscous modulus or loss modulus). During an oscillatory rheological measurement, an oscillating stress is applied and the material's response is measured in terms of G' and G".

For illustrative purposes in the following Figure 21 is reported the graph used for the identification of the gel-point for Poly(acrylic acid) (PAA) photoresin [36].

Before the gel point: G" is greater than G' , indicating a predominantly liquid behavior. At the gel point: G' and G" intersect, indicating that the material has a balanced viscoelastic component. This crossover frequency is associated with the gelation point. After the gel point: G' becomes greater than G", indicating that the material has developed a network structure and behaves more like an elastic solid.

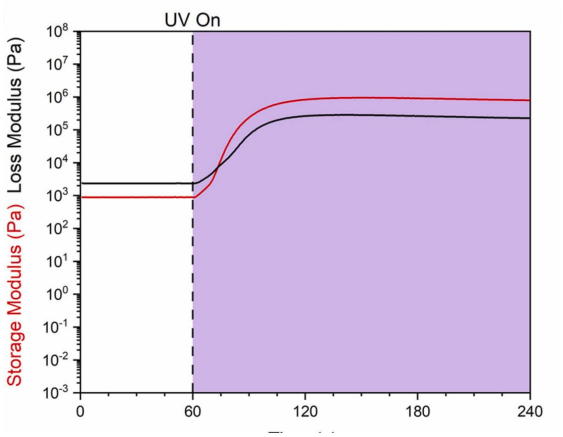

Figure 21: Photorheology data of PAA photoresin for a complete cure [36]

In this thesis, we employed acoustic characteristic analysis to generate curves describing the resin behavior, similar to the use of rheological curves to identify the gel point. This approach not only speeds up resin characterization but also enables the development of a more compact ultrasound-based device that can be directly integrated into the DLP printer. Integrating a device within the same printer that allows for autonomous characterization of the resin will enable much faster identification of the optimal combination of printing parameters (such as light intensity, exposure time, layer thickness...) for the resin being used.

4.4 Experimental setup

The first step involved replicating the printing conditions typical of a conventional DLP printer within a setup enabling monitoring of the polymerization process throughout the exposure to the light source and subsequent analysis of the obtained data. The experimental setup was tailored for through-transmission propagation.

To provide an overview, Figure 23 illustrates the experimental schematic for the in-situ ultrasonic monitoring system. The setup is assembled as follows:

- Building platform/delay line (number 1 in figure 22)
- Ultrasonic transducer/probe (number 2 in figure 22)
- UV light (number 3 in figure 22)
- Pulser/receiver unit (Advanced OEM Solutions)
- Computer for signal processing

Figure 22: Real experimental setup used

To monitor the polymerization process using the ultrasonic method, a transducer holder (figure 24) is designed, 3D printed and mounted under the build platform, where the ultrasonic transducer is fixed for performing the experiments. The transducer is placed such that it comes in contact with the metallic delay-line. An acoustic couplant gel is used for ensuring good wave transmission. Delay-line is also utilized as the build platform, and the resin specimen is directly on the surface of the delay-line as shown in Figure 23. The delay-line (building platform) has 1 cm thickness and it is made of aluminum.

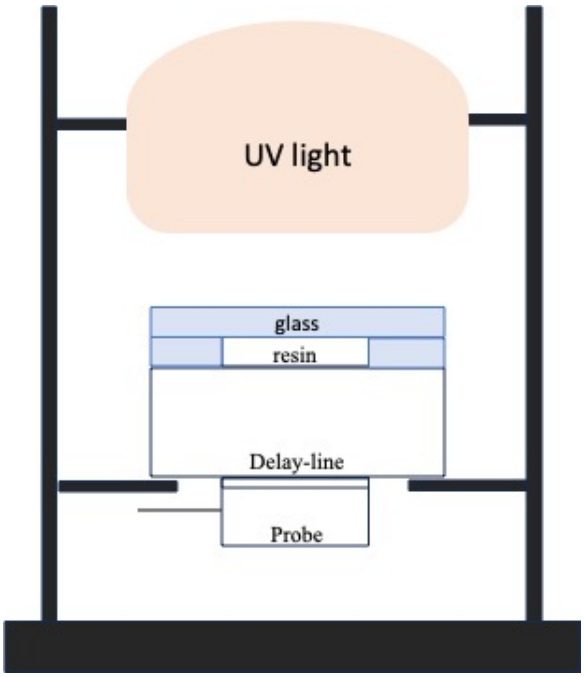

Figure 23: Experimental setup schematic configuration

In order to avoid any variation in the thickness of the resin specimen for different experiments and to isolate the outer surface from contact with oxygen, a glass slide with a thickness of 1 mm was placed on top of the resin (as shown in the figure 23), supported by two glass slides of the same thickness to create a chamber with a thickness of 1 mm in which to place the polymerizing resin.

The probe used serves as both transmitter and receiver of the ultrasonic signal. All measurements were performed using one multielement probes (Imasonic SAS, France) driven by a programmable multi-channel electronics (Advanced OEM Solutions, WestChester, USA). The probe has a linear array of 64 elements, with the following features: elementary pitch: 0.25 mm; inter elements space 0.05 mm; width of the elements: 10 mm and totale active length: 15.95 mm. The transducers operated at a central frequency on $f_c = 10$ MHz.

The probe emits a signal at its central frequency (10 MHz), generating longitudinal waves that propagate through the delay-line, the resin sample and the glass slide. The signal reflects at various interfaces, generating echoes, which are subsequently captured by the probe. To ensure optimal acoustic transmission, a thickness of 1 mm was chosen for the resin sample. The signal post-processing is then performed using MATLAB, either online or offline as required.

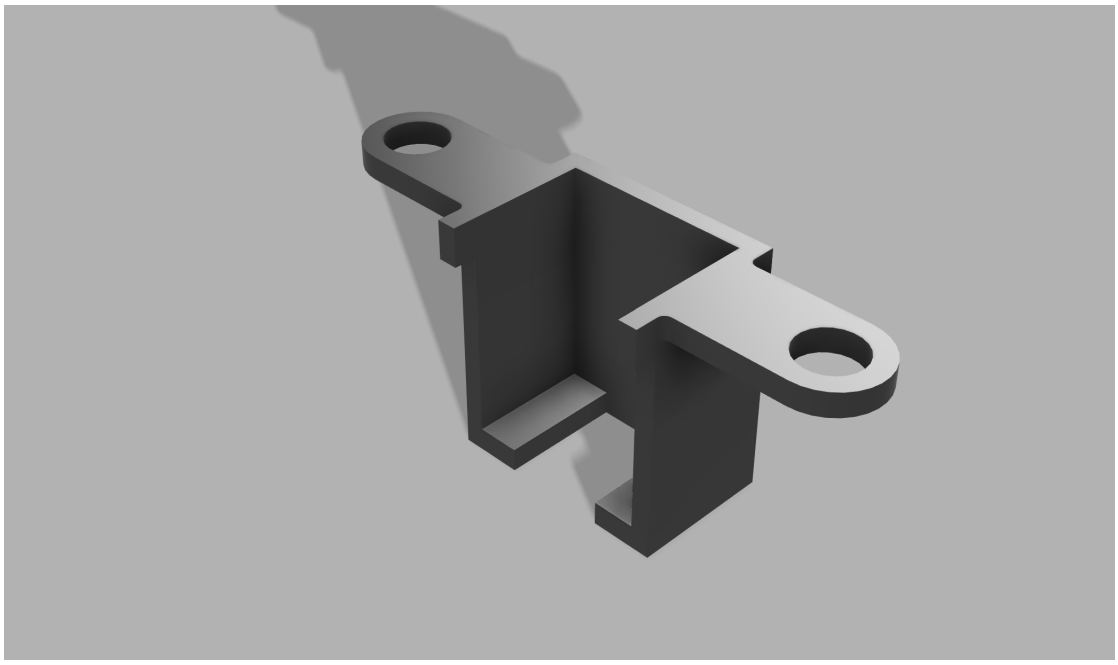

Figure 24: support designed and 3D printed to hold the transducer

5 Results and discussions

The experimental work, being conducted with the ultrasonic setup realized in the laboratory, has been focused on monitoring the phase transformations that occur during the exposition of the photopolymers at the UV light. In these measurements, the total duration of the experiment was 300 seconds, but the actual exposure time of the resin to UV light was 270 seconds (since the light is turned on after 30 seconds). Not knowing the power of the UV lamp used, it was decided to place it at the minimum possible distance and maintain a very long exposure time to ensure complete polymerization of the resin.

As an example, the figure 25 shows the signal obtained from the probe during the monitoring of polymerization. The signal at the beginning of the polymerization is shown in blue, while the signal acquired when the resin is already solidified is shown in red. It can be seen that the main peak (indicated in the figure 25 with the number 1) decreases due to the change in the reflection coefficient at the interface between the resin and the delay line. It can also be noted that the resin echo (indicated in the figure 25 with the number 2) shifts to the left because, as it solidifies, the wave propagation speed increases, and consequently, the peak arrives earlier.

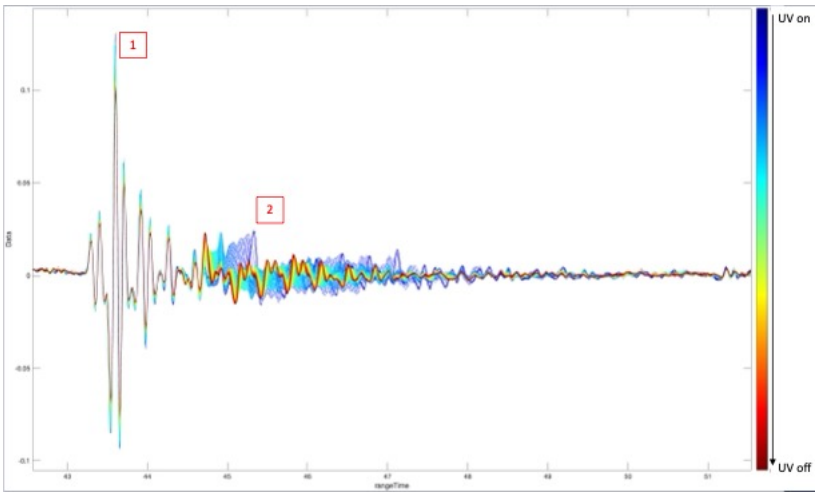

Figure 25: signal obtained from the probe during the monitoring of polymerization. 1) peak of delayline; 2) peak of resin

In Figure 26 , the curve of the ultrasonic wave propagation speed during polymerization is shown, extracted through the calculation of the time of flight (as illustrated in paragraph 3.3.1). The first thing to notice is that a sigmoid shape is obtained, the same shape as the rheological curve shown in paragraph 4.3.

The curve is characterized by three zones that can be associated with three different stages of the crosslinking reaction. In the first stage of the cure, the velocity is nearly constant because the resin is still in the liquid state and has not yet developed a viscoelastic character.

The second zone of the velocity curve starts after turning on of the UV light, when the ultrasound velocity increases rapidly due to the formation of microgel domains large enough to produce a measurable viscoelastic response to ultrasonic waves.

The third zone of the velocity curve is characterized by a progressive decrease of

the rate of change of the longitudinal velocity, which converges asymptotically to a plateau value. This zone corresponds to the vitrification stage, where a large increase in the crosslinking density with a concomitant reduction in chain mobility within the molecular network occurs. As a consequence, the crosslinking reaction becomes diffusion controlled resulting in a freezing of the network structure, whereby stable values for sound velocity are achieved [21].

The attenuation, as reported in Figure 27, remains constant before the UV light and then exhibits a very rapid increase fol-lowed by a peak and a slow decrease. After that, the rate of change of the attenuation decrease which converges asymptotically to a plateau value.

The same trend observed is also evident in the measurements conducted on PEGDA resin showed in figures 28 and 29. During the initial stage of the crosslinking process, the propagation velocity remains nearly constant, reflecting the liquid state of the resin, which has not yet developed viscoelastic properties. Upon the activation of UV light, a rapid increase in propagation velocity is observed (figure 28). In this phase, the dissipation also increases rapidly (figure 29).

The third zone of the propagation velocity curve shows a progressive decrease in the rate of change, asymptotically converging to a plateau value, indicative of the end of the polymerization. Similarly, the dissipation tends to stabilize at a constant value, reflecting the reduced chain mobility and the diffusion-controlled nature of the crosslinking reaction. These parallel behaviors in the propagation velocity and dissipation measurements highlight the complexity and interconnected nature of the structural transformations occurring in PEGDA resin during the crosslinking process.

Other speed and dissipation curves were subsequently generated by changing the UV source. For these additional experimental tests, the Spot light source (L9566-03 (Vis)) was used because its calibration curve is known. For the polymerization of the BioMed resin, the source was placed at a distance of 20 cm from the resin sample, resulting in an ultraviolet radiation intensity of 4.2 mW/cm^2. The results are reported in figures 30 and 31.

It can be observed that the total duration of the experiment, in this second measurement, was reduced from 300 seconds to 70 seconds, with the actual exposure time of the resin to UV light being only 60 seconds (since the light is turned on 10 seconds after the measurement starts). This reduced exposure time and the low intensity of the ultraviolet radiation slowed down the polymerization process and this can be seen from the dissipation curve, where the slope is not as steep as in the previous graphs. It is also possible to observe that the polymerization was not completed. This is evident from the final longitudinal speed value, which is lower than the data obtained in the previous measurements.

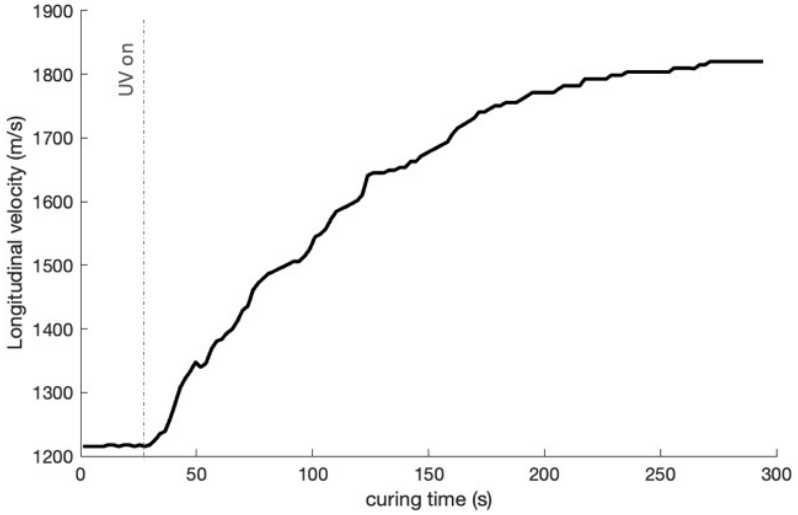

Figure 26: Longitudinal velocity for for BioMed resin measured at 10 MHz during polymerization, exposition time: 270 s

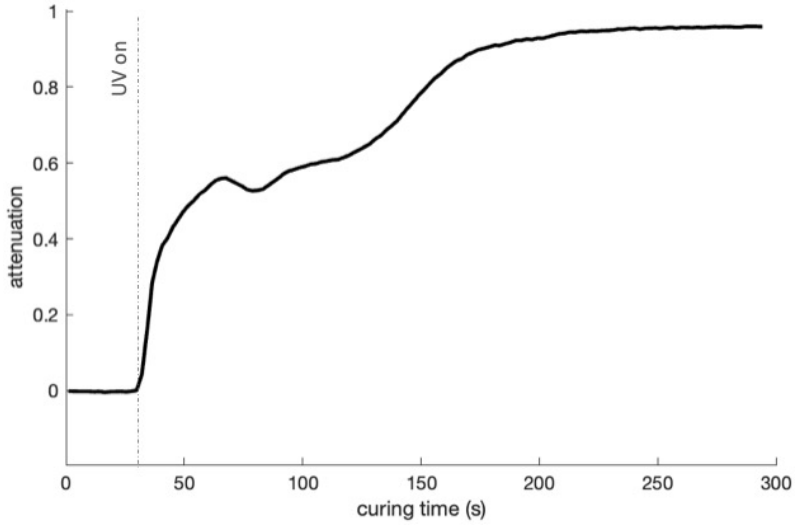

Figure 27: Ultrasonic attenuation for BioMed resin measured at 10 MHz during polymerization, exposition time: 270 s

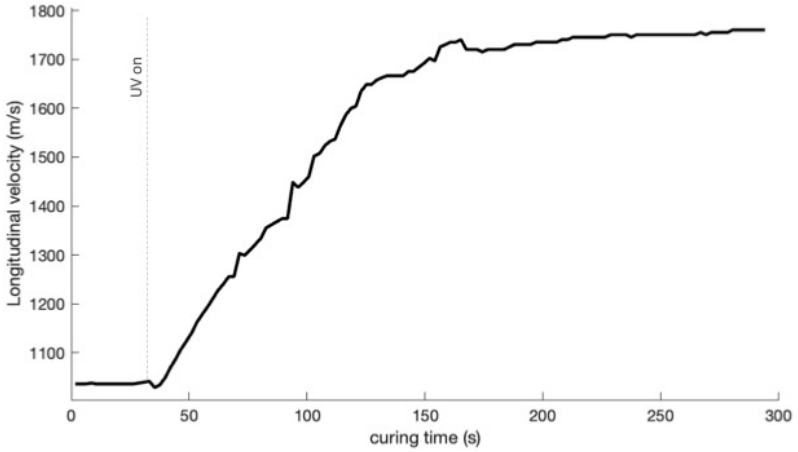

Figure 28: Longitudinal velocity for for PEGDA resin measured at 10 MHz during polymerization, exposition time: 270 s

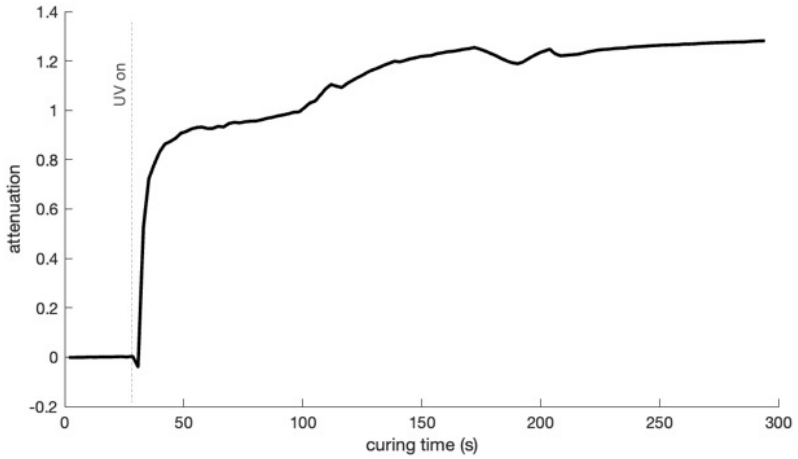

Figure 29: Ultrasonic attenuation for PEGDA resin measured at 10 MHz during polymerization, exposition time: 270 s

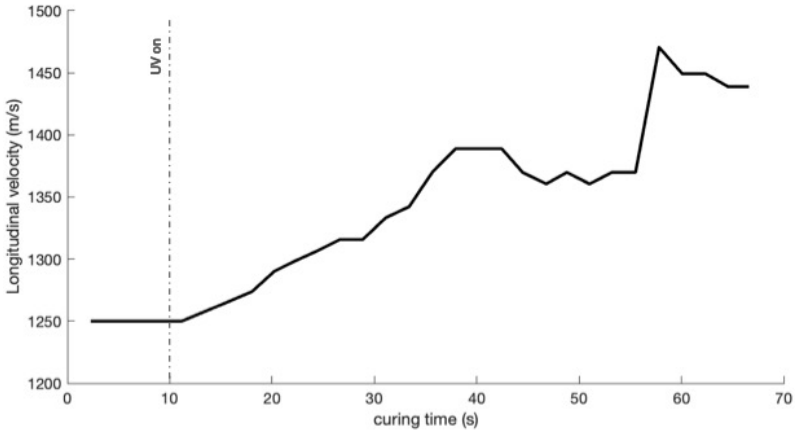

Figure 30: Longitudinal velocity for BioMed resin measured at 10 MHz during polymerization, exposition time: 60 s

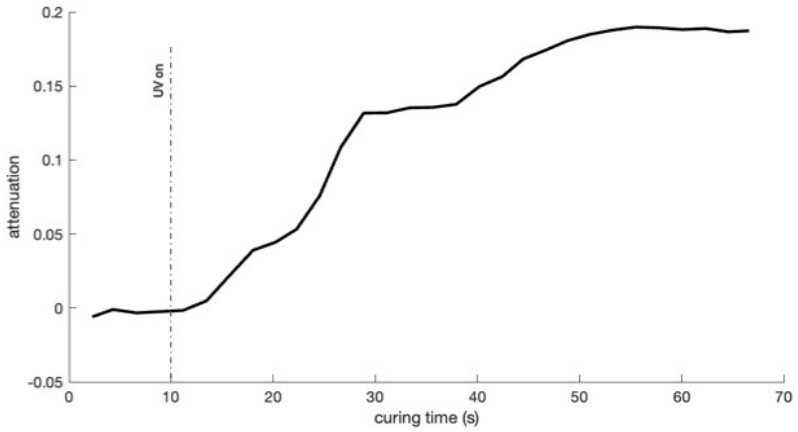

Figure 31: Ultrasonic attenuation for BioMed resin measured at 10 MHz during polymerization, exposition time: 60 s

Further analysis can be conducted by considering the amplitude variation of the first and second peaks. As previously illustrated, the first signal echo is due to the reflection of the wave with the printing platform, namely at the interface between the platform and the resin. This implies that this first echo will be sensitive to the variation of resin properties at the bottom of the layer under consideration. The polymerization of the resin will alter the reflection coefficient and consequently, the signal's amplitude. In contrast, the second peak of the signal is the echo of the ultrasonic wave that has traversed the entire resin layer and reflected at the interface with the glass slide, thus being influenced by variations in resin properties located in the upper and central part of the layer.

Observing graph in figure 32, representing the amplitude variation of the first peak in the BioMed resin, and graph in figure 33, which depicts the amplitude variation of the second peak, it is noted that due to increased dissipation after the UV lamp is turned on, both peaks decrease in amplitude. It is interesting to note that these two variations do not occur simultaneously. The second peak reduces its amplitude as soon as the UV light is turned on because the resin in the layer polymerizes first as it is closer to the lamp. The first peak, however, has a slight reduction in amplitude just after the UV light is turned on, but it begins to decrease significantly only after a certain interval of time, indicating that polymerization is not occurring uniformly within the layer. This phenomenon may be caused by the thickness of the layer being too large, which hinders the light from penetrating rapidly and uniformly into the resin.

Similar results are observed in the PEGDA resin, where the trends of the peaks are reported in graphs 34 and 35. However, in this case, it is noticeable that the resin is much more sensitive to UV and allows easier penetration. Indeed, the first peak shows a rapid decrease in its amplitude as soon as the UV light is turned on and then decreases more slowly. The second peak remains even more sensitive with a much faster amplitude variation.

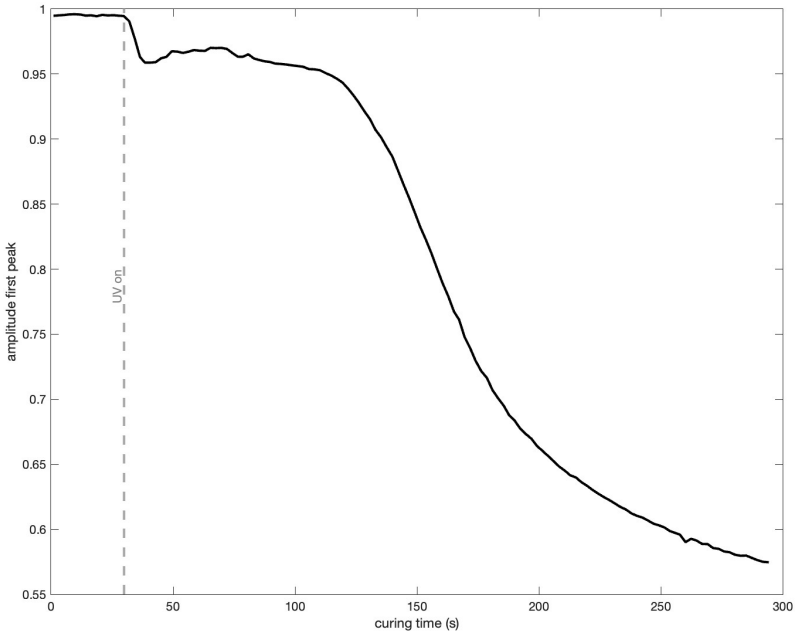

Figure 32: Amplitude first peak for BioMed resin

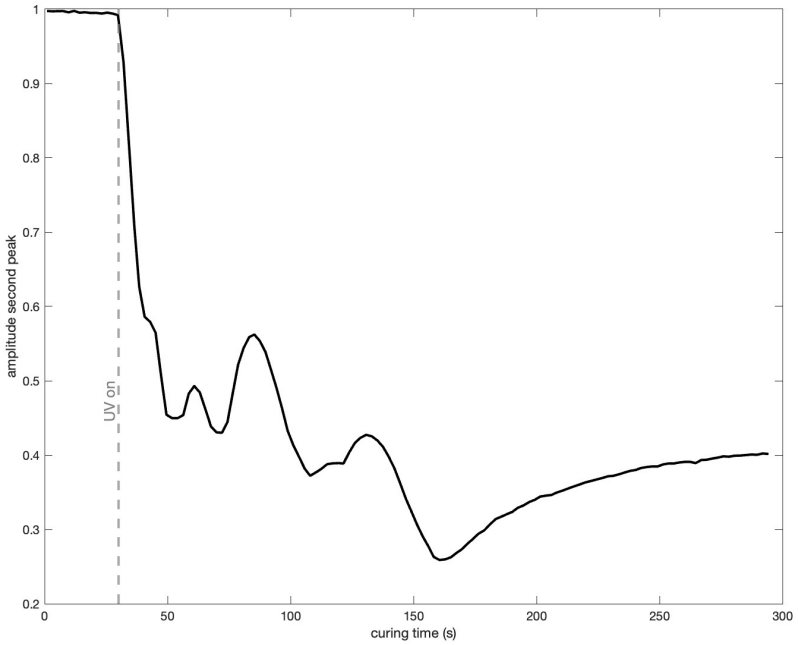

Figure 33: Amplitude second peak for BioMed resin

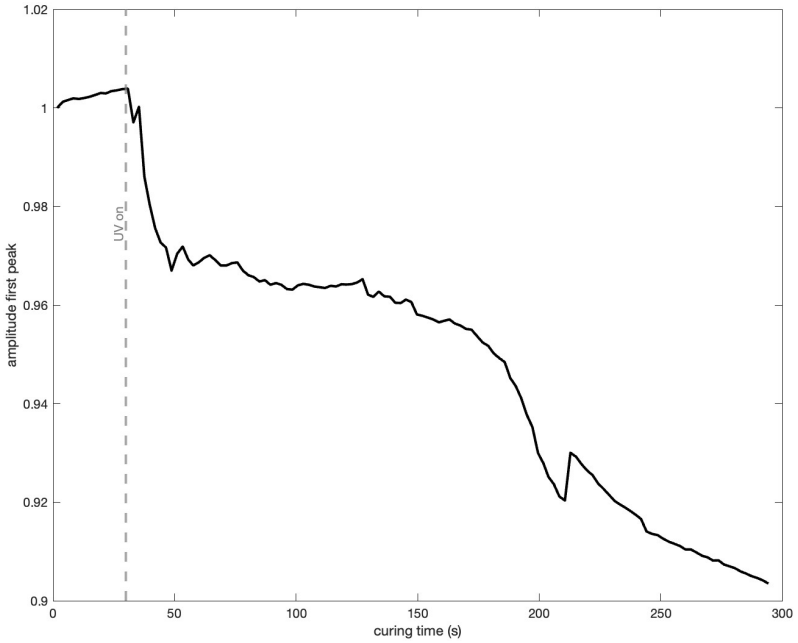

Figure 34: Amplitude first peak for PEGDA resin

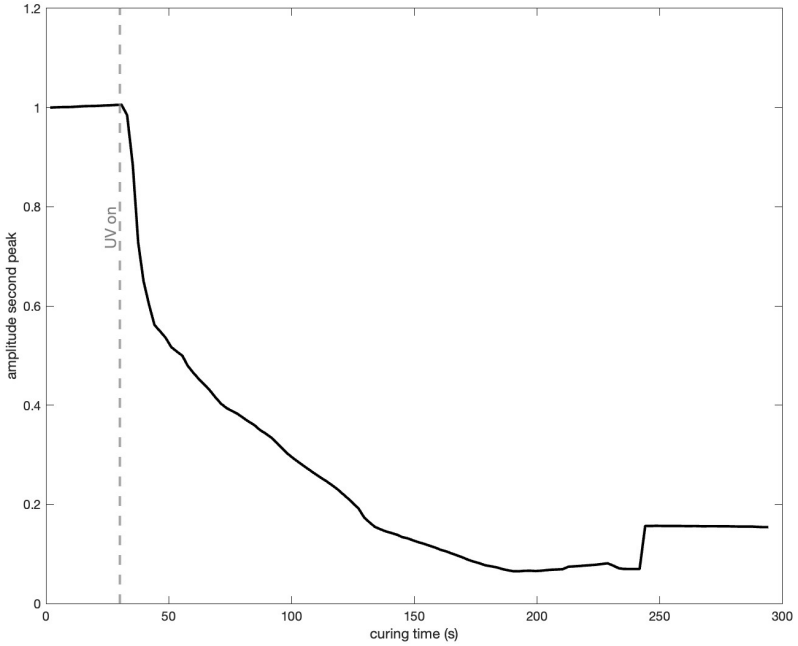

Figure 35: Amplitude second peak for PEGDA resin

6 Conclusions

This thesis aimed to conduct a preliminary study for the creation of an innovative device that allows in-situ characterization of polymer resins and real-time monitoring of the polymerization process in Direct Light Processing (DLP) printers using ultrasonic waves. The primary goal was to obtain time-dependent curves of certain ultrasonic signal parameters (propagation speed, dissipation), enabling the tracking of the resin's characteristics during the polymerization process.

The resins used were BioMed Clear (commercial resin) and PEGDA 250 as the matrix, mixed with BAPO as the photoinitiator in an amount equal to 2% by weight. The monitoring system was constructed to replicate the printing conditions inside the DLP printer, using multielement probes (Imasonic SAS, France) as the ultrasonic transmitter/receiver, capable of emitting and receiving longitudinal waves at a frequency of 10 MHz.

The signal post-processing is then performed using MATLAB, either online or offline as required. Once the experimental setup was realized, the polymerization monitoring was carried out. From the obtained signal, two quantities were extracted: the wave propagation speed and dissipation. The time-of-flight technique between two consecutive signal peaks was used to calculate the propagation speed. For extracting the dissipation information, the power spectrum technique was employed, comparing the energy of the signal echo at the start of the polymerization with that of subsequent measurements. These two quantities indicate the change in the state of the resin from liquid to solid during polymerization, as they intrinsically depend on the resin's characteristics. As illustrated in the previous chapters, the wave propagation speed is proportional to the storage modulus E':

$$c \propto \sqrt{E'}$$

while the dissipation, generally indicated for waves by α, is directly proportional to the loss modulus E'' and inversely proportional to the square root of E':

$$\alpha \propto \frac{E''}{\sqrt{E'}}$$

The information collected from the variation of the ultrasonic signal was used to make assessments on the resin's polymerization. The obtained speed and dissipation graphs are comparable to those derived from rheological studies on the resin, as they describe the behavior of the same properties. By monitoring these curves, it is possible to characterize the resin and extract information such as the gel point.

Identifying the gel point is crucial because it represents the moment when the resin transitions from a liquid to a solid state, marking the beginning of the polymer's three-dimensional network formation. Knowing this point precisely allows for the optimization of the polymerization process, ensuring that the resin attains the desired properties while minimizing defects such as incomplete polymerization or overexposure. Additionally, some defects in polymerization, such as incomplete polymerization or overexposure of the resin, can be identified. The possible future developments of the study conducted in this thesis work are:

- Implementation of a faster ultrasound signal generation and acquisition system, enabling multiple measurements per second.
- Use of a thinner resin layer to enable monitoring of resin layers during the printing process.

- Developing a mathematical model that accurately identifies and quantifies the characteristics of the resin with specific measurements.
- To implement the setup developed in this Thesis into a DLP printer.

References

[1] Salas et al. "Chemistry in light-induced 3D printing". In: *https://doi.org/10.1007/s40828-022-00176-z* (2023).

[2] Saad Alghamdi et al. "Additive Manufacturing of Polymer Materials: Progress, Promise and Challenges". In: *Polymers* 13 (Feb. 2021). DOI: 10.3390/polym13050753.

[3] Aprilia Aprilia, Naien Wu, and Wei Zhou. "Repair and restoration of engineering components by laser directed energy deposition". In: *Materials Today: Proceedings* 70 (2022). The International Conference on Additive Manufacturing for a Better World (AMBW 2022), pp. 206–211. ISSN: 2214-7853. DOI: https://doi.org/10.1016/j.matpr.2022.09.022. URL: https://www.sciencedirect.com/science/article/pii/S2214785322058163.

[4] Ali Bagheri and Jianyong Jin. "Photopolymerization in 3D Printing". In: *ACS Applied Polymer Materials* 1.4 (2019), pp. 593–611. DOI: 10.1021/acsapm.8b00165. eprint: https://doi.org/10.1021/acsapm.8b00165. URL: https://doi.org/10.1021/acsapm.8b00165.

[5] Nicholas R. Bagnall et al. "Catalytic, Sulfur-Free Chain Transfer Agents That Alter the Mechanical Properties of Cross-Linked Photopolymers". In: *Journal of the American Chemical Society* 145.26 (2023). PMID: 37341503, pp. 14202–14207. DOI: 10.1021/jacs.3c03811. eprint: https://doi.org/10.1021/jacs.3c03811. URL: https://doi.org/10.1021/jacs.3c03811.

[6] Sophian Beyerlein and Mostafa Aboushama. "Evaluation of Continuous Fiber Reinforcement Desktop 3D Printers Desktop 3D Printers Overview". PhD thesis. July 2020. DOI: 10.13140/RG.2.2.16640.87040.

[7] Tomaz Brajlih et al. "Speed and accuracy evaluation of additive manufacturing machines". In: *Rapid Prototyping Journal* 17.1 (Jan. 2011), pp. 64–75.

[8] J David N Cheeke. *Fundamentals and applications of ultrasonic waves*. CRC press, 2010.

[9] Thomas Duda and L. Raghavan. "3D metal printing technology: the need to re-invent design practice". In: *AI & SOCIETY* 33 (May 2018). DOI: 10.1007/s00146-018-0809-9.

[10] Anirban Dutta. "STUDY AND ENHANCEMENT OF ELECTROPHOTOGRAPHIC SOLID FREEFORM FABRICATION". In: (Dec. 2002).

[11] Sandeep Kumar Dwivedi, Manish Vishwakarma, and Prof.Akhilesh Soni. "Advances and Researches on Non Destructive Testing: A Review". In: *Materials Today: Proceedings* 5.2, Part 1 (2018). 7th International Conference of Materials Processing and Characterization, March 17-19, 2017, pp. 3690–3698. ISSN: 2214-7853. DOI: https://doi.org/10.1016/j.matpr.2017.11.620. URL: https://www.sciencedirect.com/science/article/pii/S2214785317328936.

[12] Gabriela E Fonseca, Marc A Dubé, and Alexander Penlidis. "A critical overview of sensors for monitoring polymerizations". In: *Macromolecular Reaction Engineering* 3.7 (2009), pp. 327–373.

[13] Formlabs. *BioMed Clear datasheet*. URL: https://formlabs-media.formlabs.com/datasheets/2001432-TDS-ENUS-0.pdf.

[14] Monica Gallo, Lydia Ferrara, and Daniele Naviglio. "Application of ultrasound in food science and technology: A perspective". In: *Foods* 7.10 (2018), p. 164.

[15] Matteo Gastaldi et al. “Functional Dyes in Polymeric 3D Printing: Applications and Perspectives”. In: *ACS Materials Letters* 3.1 (2021), pp. 1–17. DOI: 10.1021/acsmaterialslett.0c00455. eprint: https://doi.org/10.1021/acsmaterialslett.0c00455. URL: https://doi.org/10.1021/acsmaterialslett.0c00455.

[16] GEadditive. “What is additive amnufacturing?” In: *GEadditive* (2023). URL: https://www.ge.com/additive/additive-manufacturing.

[17] Ji Won Hwang et al. “Gelation and crosslinking characteristics of photopolymerized poly(ethylene glycol) hydrogels”. In: *Journal of Applied Polymer Science* 132.22 (2015). DOI: https://doi.org/10.1002/app.41939. eprint: https://onlinelibrary.wiley.com/doi/pdf/10.1002/app.41939. URL: https://onlinelibrary.wiley.com/doi/abs/10.1002/app.41939.

[18] Jean-Pierre Kruth. “Material incress manufacturing by rapid prototyping techniques”. In: *CIRP annals* 40.2 (1991), pp. 603–614.

[19] Janice K Lawson et al. “Specification of optical components using the power spectral density function”. In: *Optical Manufacturing and Testing*. Vol. 2536. SPIE. 1995, pp. 38–50.

[20] Samuel Clark Ligon et al. “Polymers for 3D printing and customized additive manufacturing”. In: *Chemical reviews* 117.15 (2017), pp. 10212–10290.

[21] Francesca Lionetto and Alfonso Maffezzoli. “Monitoring the cure state of thermosetting resins by ultrasound”. In: *Materials* 6.9 (2013), pp. 3783–3804.

[22] Francesca Lionetto et al. “Phase transformations during the cure of unsaturated polyester resins”. In: *Materials Science and Engineering: A* 370.1-2 (2004), pp. 284–287.

[23] Mario Lušić et al. “Towards Zero Waste in Additive Manufacturing: A Case Study Investigating one Pressurised Rapid Tooling Mould to Ensure Resource Efficiency”. In: *Procedia CIRP* 37 (2015). CIRPe 2015 - Understanding the life cycle implications of manufacturing, pp. 54–58. ISSN: 2212-8271. DOI: https://doi.org/10.1016/j.procir.2015.08.022. URL: https://www.sciencedirect.com/science/article/pii/S221282711500863X.

[24] Alfonso Maffezzoli et al. “Cure monitoring of epoxy matrices for composites by ultrasonic wave propagation”. In: *Journal of Applied Polymer Science* 73.10 (1999), pp. 1969–1977.

[25] Albert Migliori and Timothy W. Darling. “Resonant ultrasound spectroscopy for materials studies and non-destructive testing”. In: *Ultrasonics* 34.2 (1996). Proceedings of Ultrasonics International 1995, pp. 473–476. ISSN: 0041-624X. DOI: https://doi.org/10.1016/0041-624X(95)00120-R. URL: https://www.sciencedirect.com/science/article/pii/0041624X9500120R.

[26] Douglas L Miller et al. “Overview of therapeutic ultrasound applications and safety considerations”. In: *Journal of ultrasound in medicine* 31.4 (2012), pp. 623–634.

[27] Catalin Moldovan et al. “THEORETICAL ANALYSIS AND PRACTICAL CASE STUDIES OF SLA, POLYJET AND FDM MANUFACTURING TECHNIQUES”. In: 61 (Sept. 2018), pp. 401–408.

[28] C Moon et al. *Ultrasound techniques for leak detection*. Tech. rep. SAE Technical Paper, 2009.

[29] Rafael R Moraes et al. “Control of polymerization shrinkage and stress in nanogel-modified monomer and composite materials”. In: *Dental Materials* 27.6 (2011), pp. 509–519.

[30] Quanyi Mu et al. “Digital light processing 3D printing of conductive complex structures”. In: *Additive Manufacturing* 18 (2017), pp. 74–83. ISSN: 2214-8604. DOI: https://doi.org/10.1016/j.addma.2017.08.011. URL: https://www.sciencedirect.com/science/article/pii/S2214860417300398.

[31] Protolabs Network. “3D printing vs. CNC machining: Which is better for prototyping and end-use parts?” In: *Hubs* (2024). URL: https://www.hubs.com/knowledge-base/3d-printing-vs-cnc-machining/.

[32] Mahshid Padash, Christian Enz, and Sandro Carrara. “Microfluidics by Additive Manufacturing for Wearable Biosensors: A Review”. In: *Sensors* 20.15 (2020). ISSN: 1424-8220. DOI: 10.3390/s20154236. URL: https://www.mdpi.com/1424-8220/20/15/4236.

[33] “Phenylbis(2,4,6-trimethylbenzoyl)phosphine oxide”. In: *merck* (2023). URL: https://www.sigmaaldrich.com/FR/fr/product/aldrich/511447.

[34] “Poly(ethylene glycol) diacrylate”. In: *merck* (2023). URL: https://www.sigmaaldrich.com/FR/fr/product/aldrich/437441.

[35] Haoyuan Quan et al. “Photo-curing 3D printing technique and its challenges”. In: *Bioactive materials* 5.1 (2020), pp. 110–115.

[36] Daniel A. Rau et al. “A rheological approach for measuring cure depth of filled and unfilled photopolymers at additive manufacturing relevant length scales”. In: *Additive Manufacturing* 60 (2022), p. 103207. ISSN: 2214-8604. DOI: https://doi.org/10.1016/j.addma.2022.103207. URL: https://www.sciencedirect.com/science/article/pii/S2214860422005966.

[37] Stefano Rosso et al. “An Optimization Workflow in Design for Additive Manufacturing”. In: *Applied Sciences* 11.6 (2021). ISSN: 2076-3417. DOI: 10.3390/app11062572. URL: https://www.mdpi.com/2076-3417/11/6/2572.

[38] Abdollah Saboori et al. “Application of Directed Energy Deposition-Based Additive Manufacturing in Repair”. In: *Applied Sciences* 9.16 (2019). ISSN: 2076-3417. DOI: 10.3390/app9163316. URL: https://www.mdpi.com/2076-3417/9/16/3316.

[39] sculpteo. “What is it STL file”. In: *sculpteo* (). URL: https://www.sculpteo.com/fr/centre-apprentissage/creer-un-fichier-3d/quest-ce-quun-fichier-stl/.

[40] ASTM Standard et al. “Standard terminology for additive manufacturing technologies”. In: *ASTM International F2792-12a* 46 (2012), pp. 10918–10928.

[41] Stefano Stassi et al. “Polymeric 3D Printed Functional Microcantilevers for Biosensing Applications”. In: *ACS Applied Materials & Interfaces* 9.22 (2017). PMID: 28530385, pp. 19193–19201. DOI: 10.1021/acsami.7b04030. eprint: https://doi.org/10.1021/acsami.7b04030. URL: https://doi.org/10.1021/acsami.7b04030.

[42] Kenneth S Suslick and Gareth J Price. “Applications of ultrasound to materials chemistry”. In: *Annual Review of Materials Science* 29.1 (1999), pp. 295–326.

[43] Eduardo Umaras and Marcos S.G. Tsuzuki. "Additive Manufacturing - Considerations on Geometric Accuracy and Factors of Influence". In: *IFAC-PapersOnLine* 50.1 (2017). 20th IFAC World Congress, pp. 14940–14945. ISSN: 2405-8963. DOI: https://doi.org/10.1016/j.ifacol.2017.08.2545. URL: https://www.sciencedirect.com/science/article/pii/S2405896317334705.

[44] Mélanie W. "Le procédé DLP pour créer de meilleures pièces en caoutchouc". In: *3D Natives https://www.3dnatives.com/etec-procede-dlp-17102022/* (2022).

[45] Terry Wohlers. "Additive manufacturing advances". In: *Manufacturing Engineering* 148.4 (2012), pp. 55–63.

[46] Kaufui V Wong and Aldo Hernandez. "A review of additive manufacturing". In: *International scholarly research notices* 2012 (2012).

[47] Xiucheng Zou et al. "Internal Microdomain Regulatory Based on Upconversion Particles for Controllable Near-Infrared Photopolymerization Kinetics and Material Properties". In: *Macromolecules* 57.6 (2024), pp. 2687–2696. DOI: 10.1021/acs.macromol.4c00281. eprint: https://doi.org/10.1021/acs.macromol.4c00281. URL: https://doi.org/10.1021/acs.macromol.4c00281.